Journal of Materials Chemistry A

Accepted Manuscript

ROYAL SOCIETY OF CHEMISTRY

www.rsc.org/materialsA

Journal Name

RSC Publishing

ARTICLE

Simultaneous sulfur doping and exfoliation of graphene from graphite using electrochemical method for supercapacitor electrode materials†

Cite this: DOI: 10.1039/x0xx00000x

Received 00th January 2012,
Accepted 00th January 2012

DOI: 10.1039/x0xx00000x

www.rsc.org/

Nazish Parveen,[a] Mohd Omaish Ansari,[b] Sajid Ali Ansari,[a] and Moo Hwan Cho*[a]

Doping with hetero atoms has become a significant strategy for modifying the electronic properties and enhancing the electrochemical properties of graphene (GN). In this study, an environmental friendly, economical and facile one pot electrochemical method was developed to synthesize sulfur-doped graphene (S-GN). Sodium thio Sulphate ($Na_2S_2O_3$), in addition to acting as a sulfur source, also catalyzed the exfoliation process, resulting in sulfur-doped GN structures. The exfoliation of graphite to GN and sulfur (S) doping occurred simultaneously resulting in well dispersed S-GN frameworks. Transmission electron microscopy and high-resolution transmission electron microscopy revealed the presence of the heteroatom in S-GN, and X-ray photoelectron spectroscopy confirmed the high S content (3.47%), as well as the existence of high-quality sulphureted species (mainly as C–S–C–). The incorporation of S species in the GN during the exfoliation possess modified the surface chemistry of carbon in the GN. The electrochemical performance of the as-prepared S-GN electrode exhibited a high specific capacitances of 320 Fg^{-1} at a current density of 3 A g^{-1} and excellent cycling stability up to 1500 cycles as well as high energy density of 160 W h kg^{-1} at a power density of 5161 W kg^{-1} in an aqueous electrolyte.

Introduction

Graphene (GN) has attracted considerable attention in many research areas because of its unique two-dimensional structure, high conductivity and stability, and has been evaluated for use in electronics,[1,2] catalysts[3,4] supercapacitors, and lithium ion batteries.[5] Considerable work has been done on controlling the morphology of GN, such as three dimensional GN, zero dimensional GN, activated GN, GN-assembled foam, GN paper, GN fiber, and GN-based hydrogel, by different methods for advanced applications. As a result, the performance of GN-based materials for electrodes in supercapacitor applications has been improved.[5]

Other than a controlled morphology, another effective and simpler way to improve the capacitive performance of GN is the introduction of a heteroatom in the GN frameworks. The introduction of heteroatoms, such as nitrogen (N), phosphorous (P), boron (B), sulfur (S) etc. in carbon materials can improve the surface and bulk properties of GN significantly and may extend its applications to many fields, such as lithium-ion batteries, supercapacitors, catalyst support, superconductors, and electro catalysts for the oxygen reduction reaction.[3,6] As graphene oxide (GO) or GN inevitably contains oxygen groups, after doping with heteroatoms, some oxygen groups and some carbon atoms are replaced by these heteroatoms.[2] These heteroatoms create defects in GN that are responsible for the changes in the property of GN.

Heteroatom (N, B, S, and P) doping in GN has been used as a promising support material for capacitor applications because of its large surface area (theoretical specific surface areas of GN ~2600 m^2g^{-1}), high conductivity (10^3-10^4 S/m), good chemical and electrochemical stability, and low cost.[7,8,9] Theoretical and experimental studies have shown that doping GN with heteroatoms atoms, such as N, B and S, can modify its electronic properties and chemical reactivity, and may give rise to doped GN with hitherto unreported properties.[1,8,9] Among the different heteroatoms, doping GN with sulfur has been studied intensively over the last few years.[1,4] Doping GN with S atoms is of particular interest because the resulting materials are expected to have a wider band gap due to the electron withdrawing character of S. Previous studies have produced elemental sulfur-graphene composites by mechanically mixing the individual components or heating graphene with benzyl disulfide,[10,11] where the formation of sulfur-epoxy bonds in graphene was proposed to occur.[12] Recent studies have shown that S-doped carbon materials, such as activated carbon[13,14] CNT and GN[15,16], can be used as a promising material for supercapacitor applications. Chen et al.[15] reported sulfur-doped GN hollow nano-spheres by annealing of GO and SiO_2 nanoparticles with dibenzyl disulfide for supercapacitor applications. Thus, there appears to be scope for further studies of S-doped GN microstructures, which may be used in advanced applications.

A lot many emerging and efficient applications have been reported by various workers for the s-doped GN for example metal free cathode catalyst for oxygen reduction, supercapacitor applications, fuel cell, Li–S batteries etc.[8,9,16] therefore the possibilities and the applications can be huge. However, most of these syntheses are multistep process, which increases the cost of production as well as agglomeration formation occurs during fabrication process. Therefore, to overcome from the agglomeration problem, single step synthesis is needed for various application processes.

This paper reports the synthesis of sulfur-doped graphene (S-GN) by an electrochemical exfoliation method. In this process, the graphite sheet was simultaneously exfoliated and doped with S to generate S-GN. A combination of the H_2SO_4+$Na_2S_2O_3$ electrolyte system was used for the bulk production of S-GN. In the electrolyte, $Na_2S_2O_3$ act as a sulfur source and also catalyzed exfoliated process. A systematic study of the efficiency of the exfoliation process was conducted to determine the quality of the processed S-GN. The materials were characterized and used further as an electrode material for supercapacitor applications in a 3M KOH electrolyte solution. The as-synthesized S-GN electrode showed high specific capacitance, outstanding cyclic stability up to 1500 cycles as well as high energy and power density in the KOH electrolyte.

Experimental

Materials

Graphite rods (10 cm x 0.5 cm) for the synthesis of the S-GN were obtained from KOMAX, South Korea. Sodium thiosulfate ($Na_2S_2O_3$), sulfuric acid (H_2SO_4) and ethanol were purchased from Duksan Pure Chemicals, Co. Ltd. Korea. The water used in these experiments was de-ionized water obtained from a PURE ROUP 30 water purification system.

Methods

The microstructures of GN and S-GN were examined by field emission transmission electron microscopy (FE-TEM, Tecnai G2 F20, FEI, USA) and atomic force microscopy (AFM, The Netherlands). Phase analysis was performed by X-ray diffraction (XRD, PANalytical, X'Pert-PRO MPD, Netherland) using Cu Kα radiation (λ = 0.15405 nm). Raman spectroscopy was recorded on a Lab Ram HR 800 UV Raman microscope (Horiba Jobin-Yvon, France, λ = 514 nm) at KBSI, Gwangju Center, South Korea. The textural properties were measured by a N_2 adsorption-desorption method using a volumetric gas adsorption apparatus (ASAP 2020, Micromeritics Inc. USA). The chemical state and surface composition was analyzed by X-ray photoelectron spectroscopy (XPS, ESCALAB 250 XPS system, Thermo Fisher Scientific, UK) using a monochromatized Kα x-ray source (hν = 1486.6 eV). Electrochemical studies, such as cyclic voltammetry (CV) and galvanostatic charge/discharge (CD), were carried out using a potentiostat (Versa STAT 3, Princeton Research, USA).

Electrochemical synthesis of GN and S-GN

For the synthesis of GN and S-GN by the electrochemical exfoliation method, a graphite rod was used as both the anode and cathode materials in the working cell. The electrolytic solution used in the exfoliation process consisted of $Na_2S_2O_3$ + H_2SO_4 dissolved in H_2O; the total solution volume was 1 liter. The distance between the two graphite rods was kept to ~2 cm throughout the electrochemical process. Electrochemical exfoliation was carried out by applying a positive voltage (5.0 V) to the graphite electrode. The entire process was done under ultra-sonication bath conditions. Immediately after the reaction commenced, the solution gradually turned a grey color and finally to an intense black. The graphite anode dissociated constantly to flaky GN and exfoliated graphite sheets throughout the course of the reaction, and settled at the bottom of the bottle. After 3 hours, the dissociated exfoliated graphite sheet was filtered under suction, washed with excess water and ethanol to remove the impurities. Subsequently, the prepared S-GN was dried at 80 °C, further heated to 120 °C for 6h and stored in a desiccator for further experiments. GN was prepared similarly in the absence of $Na_2S_2O_3$. As a control experiment, different weight ratio of $Na_2S_2O_3$ to H_2SO_4 with 1:1 and 5:1 were used in the electrolyte solution for the exfoliation of S-GN. However, very slow rate of exfoliation was observed in all the cases.

Electrode preparation and electrochemical measurements

All electrochemical measurements were performed using a potentiostat Versa STAT 3, Princeton Research, USA. The working electrode was prepared by casting a nafion-impregnated sample on a carbon paper electrode with a surface area of 1 cm^2. Typically, 2 mg of GN and S-GN were dispersed in 1 mL of an ethanol solution containing 5 μL of a nafion solution in an ultrasonic bath for 20 min, which was then coated on carbon paper. The electrochemical performance was examined using a three electrode system. The electrochemical performance of the working electrode was studied by CV and CD in a 3M KOH electrolyte solution for the electrochemical studies. GN and S-GN coated carbon paper, Pt gauze and AgCl/Ag were used as the working, counter and reference electrodes, respectively, during the electrochemical process.

Results and discussion

Proposed mechanism of the electrochemical synthesis of sulfur doped graphene (S-GN)

In a GN, two types of bonding, σ-bonding and π-bonding, are observed in a rigid hexagonal framework constructed of delocalized π-bonds and C-C σ-bonds. A previous study reported that the aromaticity in GN is localized with π-electrons located in the hexagon ring.[12] Generally, when doped with a heteroatom, the rigidity of the GN is destroyed and defects are induced. In the present case, the exfoliation of graphite to GN and its simultaneous doping with S atoms by electrochemical doping results in some of the C atoms being replaced with S atoms, which result in structural distortions in GN (Fig. 1).

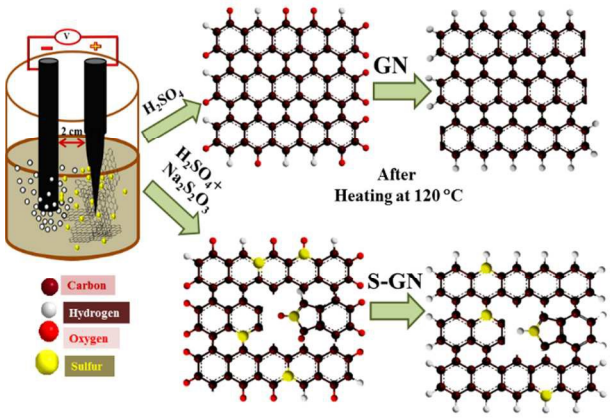

Fig. 1 Schematic diagram of the synthesis procedure and proposed atomic level schematic diagram of GN and S-GN.

Sulphate ions have been reported to accelerate the exfoliation of graphite due to the lower reduction potential of SO_4^{2-} to generate SO_2 gas[17] and produce highly dispersed GN flakes.[18] Therefore, in the present study a unique combination of H_2SO_4+$Na_2S_2O_3$ electrolyte was used for the synthesis of S-GN and H_2SO_4 for GN exfoliation. As soon as the voltage was passed, exfoliated graphite sheets were obtained readily within 5 min which settled at the bottom of the electrolytic cell. Two controlled experiments were also performed with different ratio of the $Na_2S_2O_3$ in the electrolytic solution (H_2SO_4+$Na_2S_2O_3$) and in all the cases slow rate of exfoliation was observed. In the electrolytic cell, when a voltage is passed during the dissociation process, an aqueous solution of H_2SO_4 and $Na_2S_2O_3$ dissociates to form ions in the electrolyte that can intercalate into the graphite sheets. At the same time, when the graphite rod exfoliates into the GN, the sulfur atoms replaced some of the carbon atom and few of the S atoms also attached to the GN by an electrostatic interaction with the oxygenated functional groups. These oxygenated functional groups provide active sites to attack the sulfur atom in the GN and form a C-S bond. This leads to the formation of defects and destroys the aromaticity of GN. Fig. 1 presents the suggested doping process. The reduction of water molecules in the form of OH^- ions also acts as a strong nucleophile in the electrolyte.[19] All the ionic species in the electrolyte attack the edge and grain boundaries of the graphite sheet,[20] which also helps accelerate the exfoliation process.

Another process in the cell is the self-oxidation of water and other oxidation processes taking place in the system, which produces gases, such as O_2, SO_2, etc.[20] These gases apply large forces to the graphite layers, which separate the loosely bonded graphite layers. The unique combination of the electrolyte for the synthesis of S-GN not only acts as a doping material, it also catalyzes the exfoliation process. For the exfoliation of GN, the same condition was used except that $Na_2S_2O_3$ was not added to the electrolytic solution.

Morphological studies

Morphology of the as synthesized GN and S-GN were investigated by TEM, HRTEM and AFM. GN and S-GN were coated on a carbon-coated Cu TEM grid for the analysis. Fig. S1 shows TEM images of GN and S-GN. In Fig. S1a GN shows transparent sheets with wrinkled and folded features; while in the case of S-GN (Fig. S1b), small black dots can be seen on the transparent sheet, indicating the presence of some impurities (i.e. S atom) in GN. HRTEM with elemental mapping was performed to confirm the presence of S species in the GN. From Fig. S2 HRTEM clearly showed that most of the GN and S-GN were 2-3 layered. In the case of S-GN, the TEM and HRTEM showed some randomly distributed black regions. From Fig S1, the sizes of these black regions were in the range of 4-6 nm. The S domains were confirmed by HRTEM and elemental mapping. By observing the lattice structures in Fig 2a, it appears that a small number of S atoms aggregated in the black regions. In addition Fig 2(b-c) clearly shows the lattice fringes of the S atom in the S-GN, which creates large defect regions in the S-GN during the synthesis process. The energy dispersive X-ray (EDX) spectrum of the S-GN in Fig. S3 also confirmed the presence of S in the GN. The chemical composition of the S-GN was examined by elemental mapping from Fig. 2d-f it clearly showed the presence of C, O, and S atom, which further confirms the presence of the S atom in the S-GN.

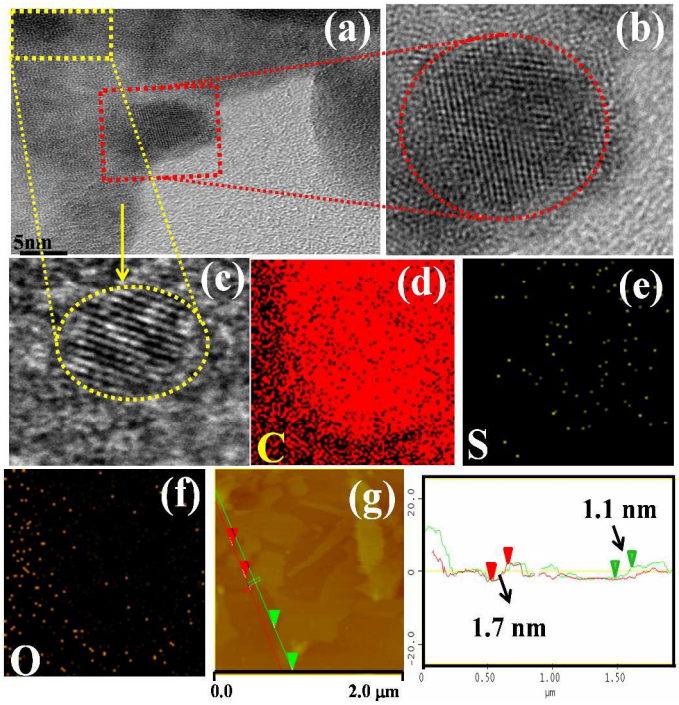

Fig. 2 (**a**) HRTEM image of S-doped GN, (**b and c**) HRTEM of selected area, (**d, e and f**) Elemental mapping of S-GN, and (**g**) AFM image of S-GN.

AFM analysis was performed to further examine the thickness of the isolated S-GN and GN. Fig. 2g and S4 show typical AFM images of the electrochemically exfoliated as-synthesized S-GN and GN deposited on the silicon substrate. The GN and S-GN surface was rough on the nanoscopic scale with some wrinkles, which might be due to the presence of functional groups. The mean thickness of GN was ~1.02 ± 1.3 nm, which increased to ~1.1 ± 1.7 nm after the electrochemical doping of S, confirming that the as synthesized GN and S-GN was 3-4 layered.

Raman analysis

Raman spectroscopy is one of the most successful tools for

examining the electronic/structural properties, thickness and defects in GN. The Raman spectra of GN and carbon-based materials generally consist of three major regions, D, G and 2D bands. The D band is assigned to the breathing mode of the sp^2 carbon atom, which is activated by the presence of defects. The G band originates from stokes Raman scattering with a single phonon (E_{2g}) emission while the other band the 2D band, is excited by a double-resonant Raman process. Fig 3a shows the comparative Raman spectra of GN and S-GN. In this case, another band, which partially merged with the G band, called the D' band (~1621 cm^{-1}), was observed and assigned to the non-zero phonon density of states above the G band in graphite.[21] After doping with S, some changes were observed, i.e., the intensities of the D band and D' band in S-GN were higher than GN due to the presence of a sulfur atom, which forms defects in GN. The G band (Fig. 3b) of S-GN was located at 1597.2 cm^{-1} (red shift of ~4 cm^{-1}) compared to GN. This red shift is an important characteristic of n-type substitutional doping in the carbon materials.[21] Seamus at al.[22] also reported that the G band shifted in S-doped multiwalled carbon nanotube compared to that in pure multiwalled carbon nanotube. In the case of S-GN due to the presence of sulfur atom, the C atoms were replaced, and formed a C-S bond, which is ~25% longer than the C–C bond.[23,24] If only the changes in the bond length are considered, the observed G band shift for S-GN would be consistent with that of B-doped GN in the fixed lattice, as reported by Terrones et al. in their B and N-doped systems.[25] Furthermore, the 2D band (Fig 3c) for GN was observed at ~2720 cm^{-1}, whereas in the case of S-GN, it was red shifted (~2710 cm^{-1}). The red shift in the 2D peak is sensitive to an increase in the number of GN layers or the doping effect. As AFM confirmed few layered GN structures, the up shift of the 2D band could be attributed to the doping effect, which is consistent with the report of the Evolution of Raman spectra for their N doped GN.[26] In Fig he I_D/I_G ratio is related to the number of defect/disordered carbon structures, and in the present case, the I_D/I_G = 0.35 obtained for GN (Fig. 3d), indicates small defects. In the case of S-GN (Fig. 3d), however, the I_D/I_G = 0.92 predicts huge defects due to the doping and lattice distortion of GN after the incorporation of sulfur atoms.

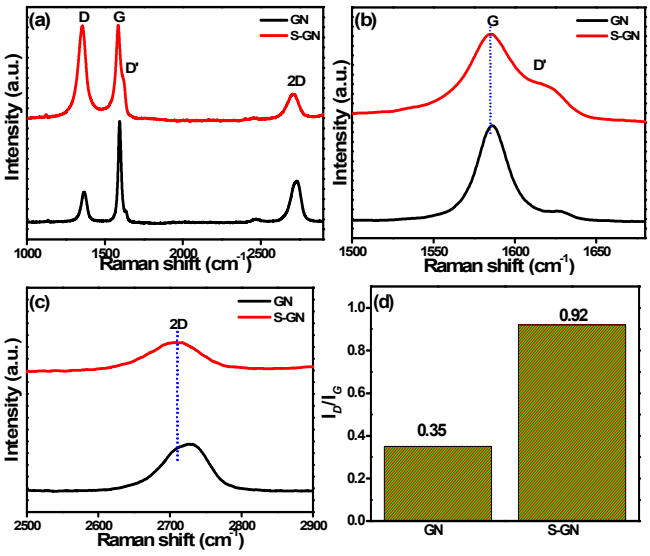

Fig. 3 (**a**) Raman spectra, (**b**) enlarge spectra of G band, (**c**) enlarge spectra of 2D band, and (**d**) I_D/I_G ratio of GN and S-GN.

XRD analysis

Fig. 4 presents the XRD patterns of GN and S-GN. The d_{002} values were calculated using Bragg's equation ($n\lambda = 2\ d \sin\theta$, where n = 1, λ is the wavelength, 1.5406 Å). An intense 002 peak in the case of GN was observed at 26.35° 2θ (d-spacing ~3.34), whereas for S-GN, it was observed at 26.19° 2θ (d-spacing ~3.39). The other 004 peak was observed at ~42.3° 2θ for GN and ~42.60° 2θ for S-GN but the noticeable difference was a much weaker diffraction peak in the case of S-GN. These results are in accordance with Wu et al.[27] regarding the effects of sulfur doping in the GN. The interlayer distance, d_{002}, increased slightly in the case of S-GN from 3.34 to 3.39 Å. In the present case, sulfur was incorporated in GN in the form of sulfur and sulfate/sulfonate groups. The diameter of a sulfur atom, 2.04 Å is larger than that of a carbon atom 1.54 Å, and sulfate/sulfonate groups are even much larger. Consequently, the interlayer distance, d_{002}, increases after the introduction of sulfur in the S-GN.

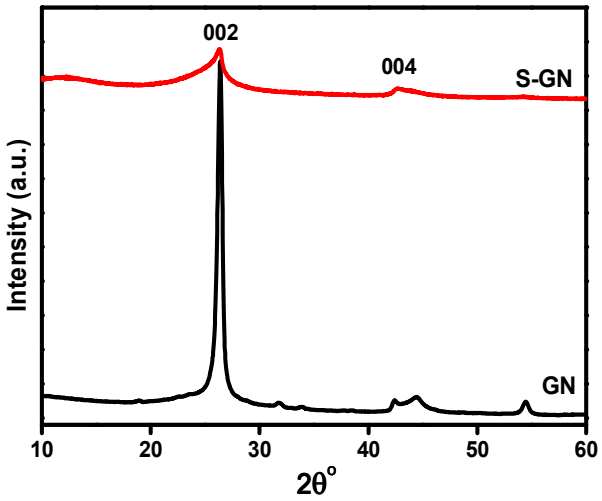

Fig. 4 XRD patterns of GN and S-GN.

XPS analysis

XPS was performed to determine the surface characterization, chemical composition, i.e., types of carbon oxygen and sulfur bonds, as well as the percentage of oxygen present in the synthesized sample. The XPS survey scans (Fig. 5a and S5) provided a complete view on the surface elemental composition of the GN, S-GN S-SN-1 and S-GN-2. The presence of sulfur in the survey spectra suggests the successful functionalization of GN by sulfur. Table S1 shows the atomic percentage of elements (C, O, and S) on the GN, S-GN, S-GN-1, and S-GN-2 surface. The atomic ratio of carbon and oxygen for GN and S-GN were 3.74 and 5.86, respectively. The higher C/O ratio in the case of S-GN indicates an ongoing reduction process during exfoliation. The changes in GN and S-GN were observed more clearly in the high-resolution C 1s core-level spectra, as shown in Fig. 5b and 5c. A typical C 1s core-level spectrum can be divided into several peaks, i.e. C=C (~284.5 eV), C-C (~285.5 eV), C-OH

(~285.9 eV), C-O (~286.6 eV), and π-π* (~290.7 eV). A drastic decrease in the peak intensity of C-O was observed from the conversion of GN to S-GN, which may have arisen from the nucleophile substitution of hydroxyl groups. Furthermore, a sharper and well-defined C=C signal in conjunction with the presence of a π-π* band on S-GN indicated the improved characteristics of conjugated/aromatic systems. The high resolution S 2p core-level spectrum was obtained to provide more details of the nature of the chemical bonding and types of sulfur present on the GN (Fig. 5d). The core-level spectrum of the S 2p was split into spin-orbit doublets of S $2p_{3/2}$ and S $2p_{1/2}$. In particular, three S $2p_{3/2}$ peaks were observed, representing the sulfur bonding of H-S-C (~163.5 eV), R-S-C (~164.5 eV) and SOx (~168.0 eV).[28] The largest peak arising from the H-S-C bond indicated the successful grafting of large thio groups into the GN carbon lattice. The R-S-C peak might be due to the presence of a small amount of hydrolyzed thiosulfate (R), while the SO_x peak could be due to the oxidation of S atoms and formation of by products, such as SO_4^{2-} and SO_3^-, which is illustrated in the inset in Fig 5d. In addition to the XPS measurements, EDX analyses highlighted the presence of sulfur in the S-GN (Fig. S3).

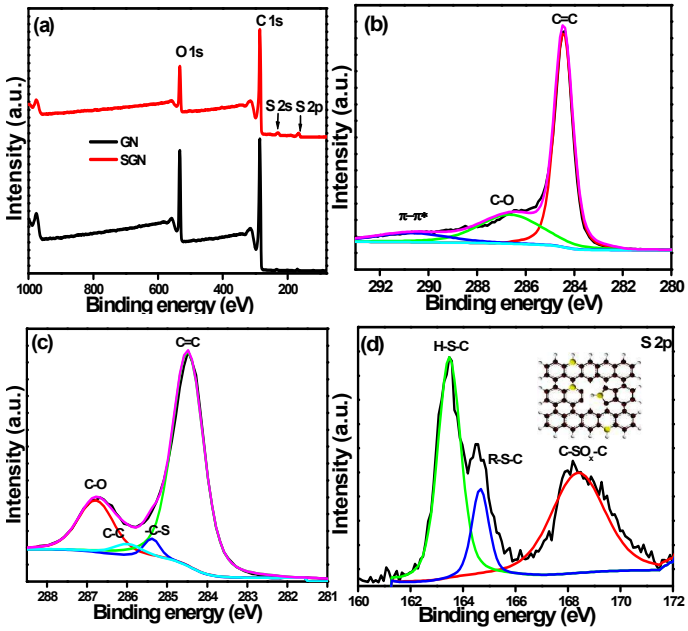

Fig. 5 (**a**) survey spectra, (**b**) High resolution C 1s core level spectra of GN, (**c**) C 1s core level spectra of S-GN, and (**d**) S 2p spectra of S-GN.

Supercapacitor performance

The electrochemical capacitance performance of the as-synthesized S-GN for supercapacitors electrode materials was evaluated by CV and galvanostatic CD measurements. CV is generally used to examine the capacitive nature of the materials. Fig. S6 shows the comparative CV voltammograms of the S-GN with different content of sulfur over the potential range of 0 to 0.8 V, and scan rates of 10 mVs^{-1}. The S-GN with 3.37 % sulfur exhibits superior capacitive performance in comparison to the S-GN with higher loading of sulfur content (S-GN-2, 8.73%). This lower performance at higher sulfur loading can be attributed to the poor ionic transportation and insufficient contact between the electrode and electrolyte.[29] A small oxidation and reduction hump at a potential of ~0.5 and 0.28 V are visible in the case of S-GN, which is related to the oxidation of sulfur to SO_4^{2-} and SO_3^- (Fig. 6a and Fig. S6).[3,28,30] In addition, CV of S-GN (Fig. 6b) and GN (Fig. S7) was also performed over the potential range, 0 to 0.8 V, and at scan rates of 10 to 100 mV/s. The introduction of sulfur functionalities, especially in thio configurations, introduces a positive charge to the neighboring carbon atoms and creates centers for the oxygen reduction reaction.[31,32] Recently, George et al.[32] analyzed the capacitive performance of sulfur-containing mesoporous carbon. They proposed that the reversible reduction of sulfones to sulfoxide and sulfoxides to hydroxylated sufoxide are responsible for the enhanced capacitive performance of relatively low surface area mesoporous carbon. In the present case, the enhanced capacitive performance of S-GN may be due to the conversion of sulfur to SO_4^{2-} and SO_3^- configurations as well as to the increased surface area (261 m^2/g) of the GN after doping with S atoms.

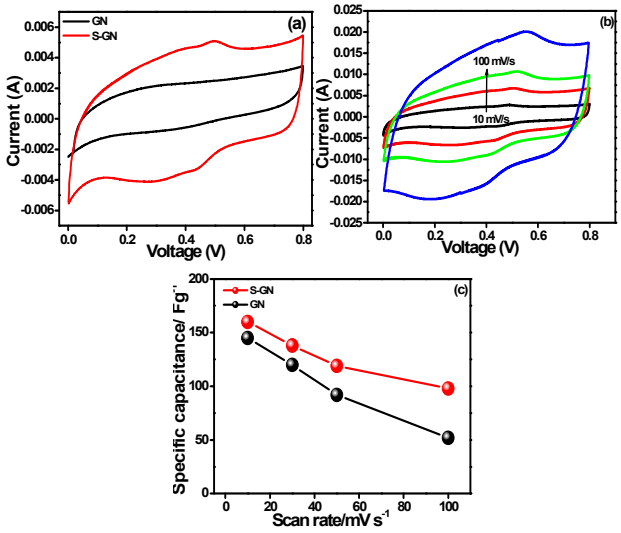

Fig. 6 (**a**) CV voltammograms of GN and S-GN at a scan rate at 20 mVs^{-1}, (**b**) CV of S-GN at different scan rates, and (**c**) specific capacitance of GN and S-GN at different scan rates.

The maximum specific capacitance of GN and S-GN obtained was 145 F/g and 160 F/g, respectively, at a current density of 10 mV/s, suggesting that S-GN has higher capacitance. Fig. 8c shows the capacitance at different scan rates; the calculations were done using equation (1).

$$CV = 2[I/\text{Scan Rate } (dv/dt)VM] \quad (1)$$

Where I is the average current during the cathodic and anodic sweep, V is the potential and M is the weight of active material coated on the carbon paper electrode. In the S-GN case, as the scan rate was increased (Fig. 6b) above 10 mV/s, the voltammograms showed slight distortion at a high scan rate of 100 mV s^{-1} due to doping with S atom, which indicates the high capacitive nature and the small equivalent series resistance with rapid charging-discharging characteristics. GN and S-GN (Fig. 6c) shows the decreasing capacitance with increasing scan rates. S-GN shows a specific capacitance of ~160 F/g at a scan rate of 10mV/s, which decreased

to ~98 F/g at 100mV/s. At very low scan rates, the capacitance is generally higher because the ions have a much longer time to enter and exist in the available electrode pores to form electric double layers, which are required to generate higher capacitance. These results suggest that the capacitive performance of the S-GN electrode was improved by doping GN with S atoms.

The galvanostatic CD curve was also measured to highlight the capacitance of the GN and S-GN. Fig. 7a and S8 shows the CD measurements of GN and S-GN recorded over the potential range, 0-0.5 V, at a current density of 5 Ag^{-1}. S-GN exhibited a longer CD time than GN, indicating the high specific capacitance of S-GN. The CD curves of GN exhibited an almost symmetrical triangular shape, whereas for S-GN, the shape was a distorted triangle with a small hump, which may be due to the conversion of S atom to SO_4^{2-} and SO_3^{-}.[28] From equation (2), the capacitance of the GN and S-GN electrodes was calculated to be 250 and 285 F g^{-1} at 5 Ag^{-1}.

$$CD = 2 (I\,dt / mdv) \quad (2)$$

Where CD is the specific capacitance (F g^{-1}), I is the charge/discharge current, dt is the time of discharge, dv is the voltage difference between the upper and lower potential limits, and m is the mass of active material. S-GN shows the specific capacitance of 320, 285 and 155 Fg^{-1} at current densities of 3, 5 and 10, respectively (Fig 7b). The high specific capacitance of S-GN might be due to its higher surface area (261 m^2/g, Fig. S9b) as compare to GN (69 m^2/g, Fig. S9a), which may offer more active sites for the electrode materials and electrolyte and can maximize the utilization of the electrode materials. The variation of the specific capacitance agrees with the values calculated from the CV. This illustrates better storage energy capacity at low current. On the other hand, for a broader context of the work, the capacitance of the material was compared with that of other reported sulfur-doped carbon material-based electrodes, as shown in Table 1. The as-synthesized S-GN showed better performance than most of the capacitors reported previously.

The cyclic stability of GN and S-GN was examined by the CD process using equation (2). Both S-GN and GN showed good cyclic stability at 5 Ag^{-1} and retained ~92% and ~ 84% capacitance after 1500 charge/discharge cycles, showing that the material has better cycling stability than that previously reported for the sulfur-doped carbon-based materials.[5,6,33] Furthermore, at higher current density (10 Ag^{-1}) S-GN (Fig. S10) retained 86% after 10,000 cycles demonstrating excellent electrochemical stability.

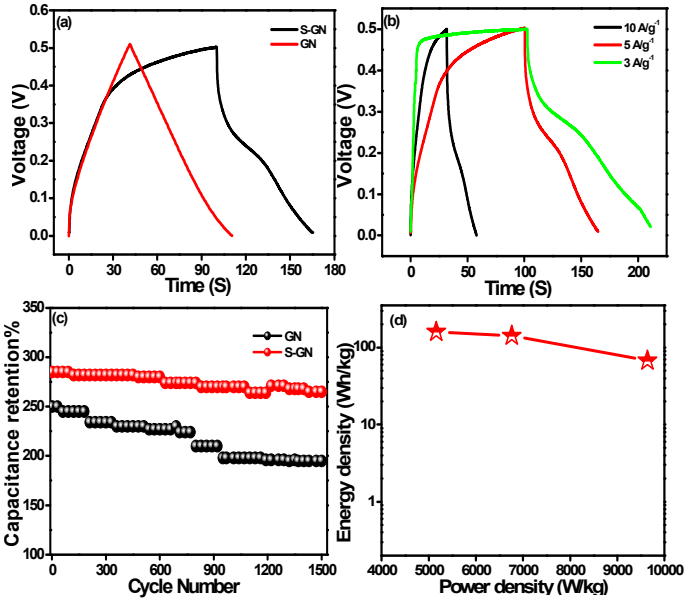

Fig. 7 (**a**) Galvanostatic CD measurement of GN and S-GN at a current density of 5 Ag-1, (**b**) CD of S-GN at different scan rates, (**c**) cyclic stability test up to 1500 cycles at a current density of 5 A g^{-1}, and (**d**) Ragone plot of S-GN.

The capacitance value of the S-GN is significantly higher than the other reported S doped carbon material for the capacitors. However, for broader context of our work, the capacitance of our S-GN is compared with the other reported S based carbon materials shown in Table 1. In addition the retention of S-GN electrode materials highlights its excellent long-term cycling stability and also suggests the high reversibility and excellent electrochemical stability of the material. Both S-GN and GN showed good capacitance behavior for supercapacitor materials. Clearly, the as-synthesized S-GN exhibited excellent rate capability. On the other hand, in the cyclic stability test of S-GN and GN, despite showing a similar trend, it exhibited significantly higher charge and discharge times, indicating that a larger number of electrons and electrolyte ions contribute to the charge and discharge processes.[20]

Table: 1 Comparison capacitance of as-prepared S-GN with other reported sulfur-doped carbon-based materials.

Capacitor	Specific Capacitance (F/g)	Current density (A/g)	Electrolyte	Retention (%)	References
S-GN	320	3A/g	3M KOH	92	Present work
S-AC	66.3	3 A/g	2M KOH	85	5
S-PCNS	312	0.5 A/g	6M KOH	97	14
S-PGHS	175	5 A/g	2M KOH	96	15
S-Containing AC	177	5 A/g	2M KOH	--	32
SAC	62.04	1.4 A/g	0.5 H_2SO_4	90	33
CGO	110	50 mA/g	6 M KOH	--	34

Fig. 7d presents the Ragone plot relating the energy density to the power density of the supercapacitor device. The specific power and specific energy were calculated from the CD curves (Fig 10b) using equations (3) and (4), respectively.

$$E=1/2(CV2) \quad (3)$$

$$P=E/\Delta t \quad (4)$$

where V is the cell voltage and Δt is the discharge time. The maximum energy density was 160 W h kg^{-1} at a power density of 5161 W kg^{-1} in 3M KOH electrolyte and an energy density of 67.5 W h kg^{-1} was maintained at a higher power density of 9541 W kg^{-1}, suggesting that S-GN has great promise for practical applications in terms of stability, cost and environment. The specific power decreased linearly with increasing specific energy for all the cells, which means that less energy is released at a higher power output.

EIS technique was further used to examine the electron-transfer properties of the GN and S-GN electrodes. Fig. 8 shows the impedance spectra of GN and S-GN electrode in aqueous KOH electrolyte. The smaller diameter of the arc in the Nyquist impedance spectra generally reflects the lower electron-transfer resistance at the surface of the electrodes and vice versa.[35-40] As compared to GN, the S-GN showed much smaller semicircular arc in the Nyquist impedance spectra, thereby indicating much lower charge transfer resistance, which might be attributed to the high electron-conductive properties of S-GN in comparison to GN. These results are also in accordance with the electrochemical properties of S-GN.

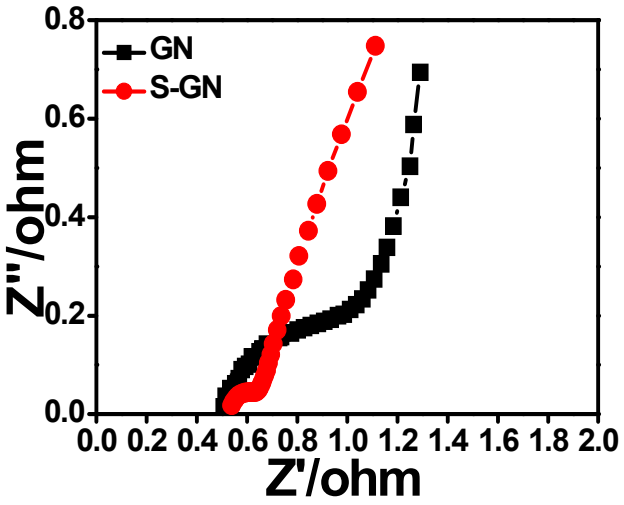

Fig. 8 Nyquist plots of GN and S-GN.

Conclusions

A simple one pot electrochemical exfoliation route was developed for the synthesis of S-GN for electrochemical storage. The proposed methodology has a number of advantages over other reported methods because it is an environmentally-friendly, single-step synthesis, and more importantly, the electrolyte acts as both a dopant for the S atom and catalyzes the exfoliation process. The exfoliation of graphite into GN and S doping occurred simultaneously, resulting in well dispersed S-GN frameworks. The structural characterization of S-GN based on XPS, elemental mapping, EDX, and Raman spectroscopy indicated a successful functionalization process. The resulting S-GN contained sulfur groups at 3.47 % based on XPS. The introduction of a S atom in GN increases the surface area of S-GN, resulting in better electrochemical performance for supercapacitor applications. The high specific capacitance of S-GN (320 Fg^{-1}) at 3 A/g, excellent reversibility with a cycling efficiency of ~92% after 1500 cycles in 3M KOH highlights the efficacy of the proposed method. The as-synthesized S-GN is expected to act as a replacement electrode material for applications in supercapacitors and opens routes for the inclusion of defects in GN by different elements for advanced applications.

Acknowledgements

This study was supported by Priority Research Centers Program (Grant No:2014R1A6A1031189), and by Basic Science Research Program (Grant No:2015R1D1A3A03018029) through the National Research Foundation of Korea (NRF) funded by the Ministry of Education.

Notes and references

[a]*School of Chemical Engineering, Yeungnam University, Gyeongsan-si, Gyeongbuk 712-749, South Korea. Phone: +82-53-810-2517; Fax: +82-53-810-463.*
[b]*Centre of Nanotechnology, King Abdulaziz University, Jeddah 21589, Saudi Arabia.*
***Email:** mhcho@ynu.ac.kr*

†Electronic Supplementary Information (ESI) available: [TEM, HR-TEM images of GN and S-GN, EDX of S-GN, AFM image of GN, XPS survey spectra and atomic % Table of GN and S-GN, CV and CD of GN, N_2 adsorption-desorption curves, comparative CV voltammograms of the GN and S-GN, Cyclic stability of S-GN.] See DOI: 10.1039/b000000x/

1. L. Zhang, J. Niu, M. Li, and Z. Xia, *J. Phys. Chem. C*, 2014, **118**, 3545−3553.
2. S. Yang, L. Zhi, K. Tang, X. Feng ,J. Maier and K. Mullen, *Adv. Funct. Mate*r. 2012, **22**, 3634–3640.
3. B. Quan, S.H.Yu, D.Y. Chung, A. Jin, J.H. Park, Y.E. Sung, Y. Piao, *Scientific reports* 2014, **4**, 5639-5639.
4. C. K. Chua and M. Pumera, *ACS Nano,* 2015, **4**, 4193–4199.
5. L. Wang, X. Li, J. Ma, Q. Wu, X. Duan, *Sustainable Energy*, 2014, **2**, 39-43.
6. M. Liu, J. Qian, Y. Zhao, D. Zhu, L. Gan and L.Chen, *J. Mater. Chem. A*, 2015, **3**, 11517-11526
7. X. Wang, X. Li , L. Zhang , Y. Yoon , P.K. Weber , H. Wang , J. Guo , H. Dai, *Science*, 2009, **324**, 768–771.
8. H. M. Jeong, J. W. Lee, W. H. Shin , Y. J.Choi , H. J. Shin, J. K. Kang and J. W. Choi, *Nano Lett*., 2011, **11**, 2472–2477.
9. Y. Zhao, C. Hu, Y. Hu, H. Cheng, G. Shi and L. Qu, *Angew. Chem. Int. Ed*., 2012, **51**, 11371–11375.
10. Y.Yan, Y.-X.Yin, S.Xin, Y.-G.Guo, L.-J.Wan, *Chem. Commun*. 2012, **48**, 10663–10665.
11. J.Z.Wang, L.Lu, M.Choucairc, J. A. Stridec, X. Xua, H.K. Liu, *J. Power Sources*, 2011, **16**, 7030–7034.
12. Z.Yang, Z.Yao, G. Li, G. Fang, H. Nie, Z. Liu, X. Zhou, X. Chen, S. Huang, *ACS Nano*, 2012 , **6**, 205–211.

13. J. P. Paraknowitsch and A. Thomas, *Energy Environ. Sci*., 2013, **6**, 2839–2855.
14. W. Deng, Y. Zhang, L. Yang, Y.Tan, M. Ma, and Q. Xie, *RSC Adv*., 2015, **5**, 13046–13051.
15. X. Chen, X. Chen, X. Xu, Z.Yang, Z. Liu, L. Zhang, X. Xu, Y. Chen and S. Huang, *Nanoscale***,** 2014, **6**, 13740–13747.
16. I. Popov, K. Bozhenko, A. Boldyrev, *Nano Res.,* 2012, **5**, 117–123.
17. F. Bech, H. Junge and H. Krohn, *Electrochim. Acta*, 1981, **26** 799–809.
18. K. Parvez, Z. S. Wu, R. Li, X. Liu, R. Graf, X. Feng and K. Mullen, *J. Am. Chem. Soc*., 2014, **136**, 6083–6091.
19. N. J. Bunce, D. Bejan, *Electrochim. Acta*, 2011, **56**, 8085–8093.
20. N. Parveen, M. O. Ansari and M. H. Cho, *RSC Adv*., 2015, **5**, 44920–44927.
21. H. Gao, Z. Liu, L. Song, W. Guo, W. Gao, L. Ci, A. Rao, W. Quan, R. Vajtai and P. M Ajayan, *Nanotechnology*, 2012, **23**, 275605–275612.
22. S. A. Curran, J. Cech, D. Zhang, J. L. Dewald, A. Avadhanula, M. Kandadai and S. Roth, *J. Mater. Res*., 2006, **21**, 1012–1018.
23. J. Wang, R. Ma, Z.Zhou, G. Liu& Q. Liu, *Scientific reports*, 2015, **5**, 9304.
24. S. A. Curran, J. Cech, D. Zhang, J. L Dewald, A. Avadhanula, M. Kandadai and S. Roth, *J. Mater. Res*., 2006, **21**, 1012.
25. M. Terronesa, A. Joriob, M. Endoc, A. M. Raod, Y. A. Kimc, T. Hayashic, H. Terronesa, J.C. Charliere, G. Dresselhausf, and M. S. Dresselhausg, *Materials Today*, 2004, **7**, 30–45.
26. Z. Zafar, Z. H. Ni, X. Wu, Z. X. Shi, H.Y. Nan, J. Bai and L. T. Sun, *Carbon*, 2013, **61**, 57–62.
27.P. Wu, S. Fang, Y. Jiang, R. Holze, *J. Power Sources*, 2002, **108**, 245–249.
28. P. A. Denis**,** *J. Phys. Chem. C*, 2009, **113**, 5612–5619.
29. W. D. Zhou, H. Chen, Y. C. Yu, D. L. Wang, Z. M. Cui, F. J. DiSalvo and H. D. Abruna, *ACS Nano*, 2013, **7**, 8801–8808.
30. W. Gu, M. Sevilla, A. Magasinski, A. B. Fuertes,and G. Yushin, *Energy Environ. Sci.,* 2013, **6**, 2465-2476.
31. X. Zhaoa, Q. Zhanga, C.M. Chena, B. Zhanga, S. Reichea , A. Wang, T. Zhang, R. Schlogla, D. S. Su, *Nano Energy*, 2012, **1**, 624–630.
32. G. Hasegawa, M. Aoki, K. Kanamori, K. Nakanishi, T. Hanada and K. Tadanaga, *J. Mater. Chem.*, 2011, **21**, 2060.
33. Y. Huang,S. L. Candelaria, Y. Li, Z. Li, J. Tian, L. Zhang, G. Cao, *J. Power Sources*, 2014, **252**, 90-97.
34. M. Seredych and T. J. Bandosz, *J. Mater. Chem. A*, 2013, **1**, 11717–11727.
35. L. F. Chen, X. D. Zhang, H. W. Liang, M. Kong, Q. F. Guan, P. Chen, Z. Y. Wu, S. H. Y. Chen, *ACS Nano*, 2012, **6**, 7092–7102.
36. W. Si, J. Zhou, S. Zhang, S. Li, W. Xing, S. Zhuo, *Electrochim. Acta,* 2013, **107,** 397–405.
37. S. A. Ansari, M. M. Khan, M. O. Ansari, M. H. Cho, *New J. Chem.*, 2015, **39**, 4708-4715.
38. S. A. Ansari, M. M. Khan, M. O. Ansari, M. H. Cho, *Sol. Energ. Mat. Sol. C*, 2015, **141**, 162–170.
39. S. A. Ansari, M. M. Khan, J. Lee, M. H. Cho, *J. Ind. Eng. Chem*, 2014, **20**, 1602−1607.
40. S. A. Ansari, M. M. Khan, M. O. Ansari, J. Lee and M. H. Cho, *J. Phys. Chem. C*, 2013, **117**, 27023−27030.

Graphical Abstract